Ref. Ares(2024)5536246 - 31/07/2024

HEFT

D4.1 Electromagnetic and Performance. Design Report of Motor for Class A+B Vehicles

Funded by
the European Union

Call	HORIZON- CL5-2020-D5-01	
GA Number	101096306	
Deliverable No.	D4.1	
Deliverable Title	Electromagnetic and performance Design report of motor for class A+B vehicle	
Deliverable Date	2024-07-24	
Contractual delivery	2024-05-31	
Deliverable Type	R	
Dissemination level	PU	
Status	V2.1	2024-07-31

Written By	Gaizka Almandoz, Aritz Egea	2024-05-31
Checked by	Iago Martinez	2024-07-12
Approved by	Javier Poza	2024-07-24

HORIZON CL5-2020-D5-01. HEFT 101096306 – Novel concept of a Low Cost, High Power Density and Highly Efficient Recyclable motor for next generation mass produced electric vehicles

Acknowledgement:

The author(s) would like to thank the partners in the project for their valuable comments on previous drafts and for performing the review.

Project partners:

1. MGEP (Mondragon Goi Eskola Politeknikoa Jose Maria Arizmendiarrieta S Coop).
2. GKN (GKN Driveline Zumaia SA).
3. GKN AIC (GKN Automotive Innovation Center - GKN Hybrid Power Ltd.).
4. MAGNETI (Magneti Ljubljana d.d.).
5. VYNCOLIT (Vyncolit N.V.).
6. IKERLAN (IKERLAN S. Coop.).
7. UNIBO (Alma Mater Studiorum - Università di Bologna).
8. KUL (Katholieke Universiteit Leuven).
9. UoN (University of Nottingham).

Disclaimer:

This project has received funding from the European Union's Horizon Europe research and innovation programme under grant agreement No 101096306. Funded by the European Union. Views and opinions expressed are however those of the author(s) only and do not necessarily reflect those of the European Union, the European Commission or the European Climate, Infrastructure and Environment Executive Agency (CINEA). Neither the European Union nor the granting authority can be held responsible for them.

1 EXECUTIVE SUMMARY 5
2 DESIGN PROCESS 6
2.1 DESIGN METHODOLOGY 6
2.1.1 Preliminary Sizing *6*
2.1.2 Optimization *6*
2.2 EVALUATION OF MOTOR PERFORMANCES 7
2.2.1 Peak Torque/Power envelopes *7*
2.2.2 Continuous Service *7*
2.2.3 Demagnetization Risk in Magnets *7*
2.2.4 Evaluation of KPIs (Key Performance Indicators) *8*
3 PRELIMINARY SIZING OF THE MOTOR 9
3.1 DESIGN CONSTRAINTS 9
3.2 DESIGN OF THE STATOR 10
3.3 DESIGN OF THE ROTOR 11
4 OPTIMIZATION OF THE ROTOR 13
4.1 DEFINITION OF THE OPTIMIZATION PROCESS 13
4.2 PARETOS OF THE OPTIMIZATION PROCESS 14
4.3 PERFORMANCE AND KPI ANALYSIS OF OPTIMIZED ROTORS 15
4.4 MINIMIZATION OF TORQUE RIPPLE IN THE V-BLOCK ROTOR 18
5 CONTINUOUS SERVICE PERFORMANCE 21
5.1 COMPUTATION OF LOSSES 21
5.1.1 Copper losses *21*
5.1.2 Iron losses *22*
5.1.3 Magnet losses *23*
5.2 COOLING SYSTEM 23
5.3 CONTINUOUS SERVICE CURVES 24
6 FINAL PERFORMANCES AND COMPUTATION OF KPIS 26
6.1 EVALUATION OF KPIS 26
6.1.1 Computation of Weight and Volume *26*
6.1.2 Evaluation of Torque and Power Densities *28*
6.1.3 Evaluation of the REE Saving *29*
6.2 FINAL PERFOMANCES 31
7 DELIVERY DEVIATIONS FROM THE INITIAL PLANNING 33
8 CONCLUSIONS 34
9 REFERENCES 35

GLOSSARY

Abbreviation/ acronym	Description
MTPA	Maximum Torque per Ampere
MTPV	Maximum Torque per Voltage
GA	Grant Agreement
KPI	Key Perfomance Indicator

1 EXECUTIVE SUMMARY

Climate change has created an increased need for innovation in various sectors, including the automotive industry. Many corporations are striving to fulfil this need by developing and producing electric cars. However, the production process remains inefficient and environmentally harmful. The EU-funded HEFT project will reverse this trend by introducing a revolutionary synchronous motor for electric cars, which will be recyclable, cost-efficient and require fewer materials while producing fewer emissions and creating novel European circular economies.

HEFT Project proposes a set of innovation challenges on electric synchronous motor configuration based on SiC inverters (direct cooling of rotor and stator, advance insulation for high voltage, multibarrier rotor topology, wave windings) and advanced materials (advanced GBD magnets, epoxy for magnet fixation, composite for motor housing, insulation resin). These innovations will result in a high-efficient and low-cost solution that will be validated on 2 motor topologies.

- Motor topology type C: Motors for C-D-E vehicle segments.
- Motor topology type A: Motors for A-B vehicle segments.

In this document the work carried out in Task 4.1 of HEFT project has been summarized. An ultra-light motor design for segment A+B is developed. The multi-layer rotor topology makes possible to reduce de usage of permanent magnet leading to an important saving in the rare earth elements. Wave winding techcnology allows to develop compact and efficient stator. End winding length is reduced and high frequency losses are reduced in the copper. Involving all these techonologies a high power density motor is developed.

In this document the following issues will be covered:

1. Design Process (Design Methodology and Procedure to motor performances evaluation).
2. Preliminary sizing of the motor.
3. Optimization of the rotor
4. Continuous service evaluation.
5. Final performances evaluation and KPIs computation.

2 DESIGN PROCESS

2.1 Design Methodology

The applied design methodology consists of 3 main stages as it is shown in Figure 1. In the first stage the stator geometry, the magnet grade, and the different rotor topologies to be considered are defined. In the second stage all these rotor topologies are sized in order to fulfil the specifications. As a result of this stage, preliminary design proposals are obtained, and finally these proposals are optimized in the third stage, applying genetic optimization algorithms.

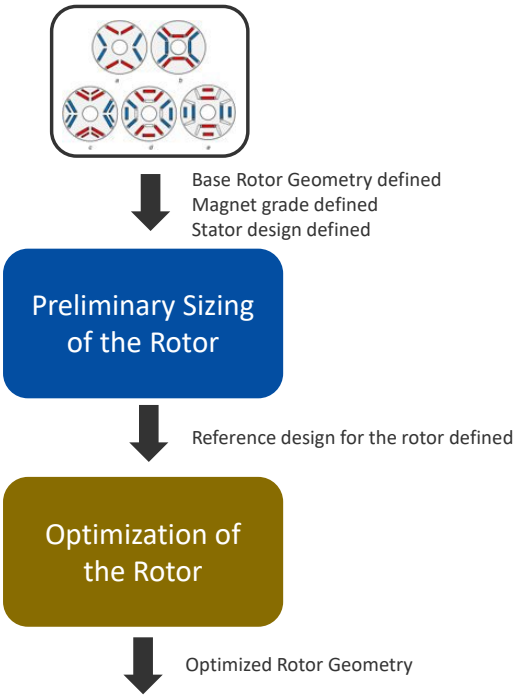

Figure 1. Flow chart of the applied design process

2.1.1 Preliminary Sizing

A first approach is carried out for each rotor topology, adjusting manually the 2D geometries and the stack length, trying to improve as much as possible the performances and the KPIs.

2.1.2 Optimization

Genetic algorithm is used to run the optimization process. The rotor geometries are parametrized. A sensitivity evaluation is carried out in order to identify the most relevant design parameters. And then these parameters are adjusted by means of a genetic optimization algorithm.

To run the optimization the next objectives have been defined:

- To maximize the power density as much as possible
- To minimize the demagnetization as much as possible, at the worst working condition (Injecting maximum current in the d-axis)

In addition, the following constraints have been considered:

- Maximum magnet mass: 1 Kg (this value is chosen according to the needed magnet saving rates)
- Meet the peak torque envelop with the maximum current

2.2 Evaluation of Motor Performances

2.2.1 Peak Torque/Power envelopes

The peak torque envelop is obtained considering the maximum current of 350A and applying the Maximum Torque per Ampere (MTPA) strategy up to the base speed. At the base speed the supplying voltage reaches the maximum allowed value (defined by the inverter, in this case 265V rms per phase), and from this speed the applied strategy is the maximum torque per voltage (MTPV). The maximum power envelop is obtained multiplying the maximum torque and the speed.

2.2.2 Continuous Service

The continuous service is defined as the steady state working point. At each specified operation speed the steady state operation mode is computed limiting the working temperatures to 180ºC for the winding and 120ºC for the magnets. As in the same way done for the maximum envelope, for the computation of continuous service working points the MTPA strategy is applied while the supplying voltage is below the maximum allowed value. In case the maximum voltage value is reached MTPV strategy is applied.

2.2.3 Demagnetization Risk in Magnets

Besides fulfilling the specified working points, the motor must withstand all working points without losing the energy stored in the magnets. The maximum torque/power envelopes are considered to be the worst operating points concerning the risk of demagnetization in the magnets. In order to assure the integrity of the magnets in the entire operating map the working point of the magnets is analysed over the peak envelop.

The characteristic curve of the magnet is considered at the working temperature. In this case 120ºC is defined as the working temperature to evaluate the demagnetization. The demagnetization knee point over the characteristic curve of the magnet must be considered. In case of magnets grade N38H, the knee point is situated at $B = 0.37\ T$ (see Figure 2).

It must be assured that the working point of all magnets is above this knee point over all peak torque envelop to avoid the risk of demagnetization.

In addition, a more restrictive conditions are included for the comparison of different rotor topologies. The energy loss of the magnets is evaluated in the situation that all current is injected in the d-axis. It is not expected that the magnets do not losses any energy in this extreme operation mode, but probably the magnets will get partially demagnetized. The purpose of this analysis is to evaluate the most robust rotor topology against the risk of demagnetization of magnets.

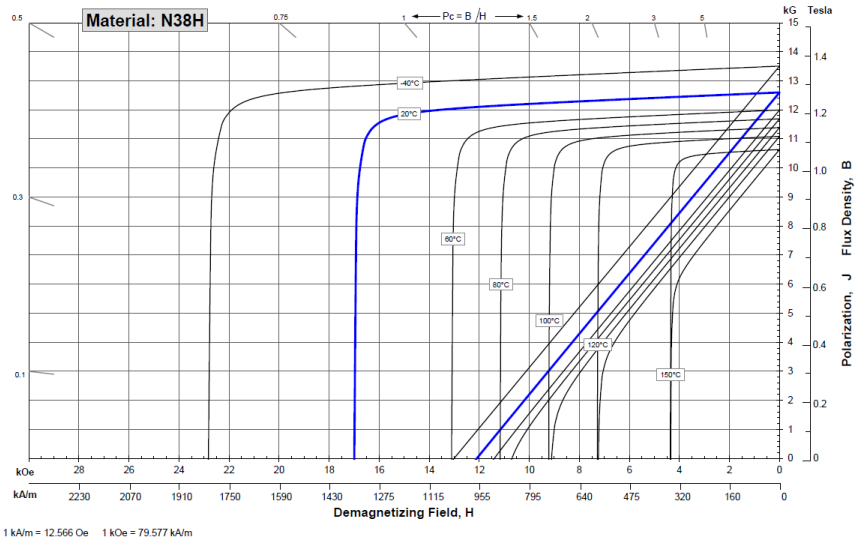

Figure 2. Characteristic curves of magnets N38H at different working temperatures

In Figure 3 the result of the demagnetization analysis is shown. In this particular case, almost the entire magnet region in the upper layer is below the knee point (see non-coloured region inside magnets). That means that the upper layer magnets are get completely demagnetized. The energy loss is computed as the percentage of the magnet region working below the knee point with respect to the overall magnet region.

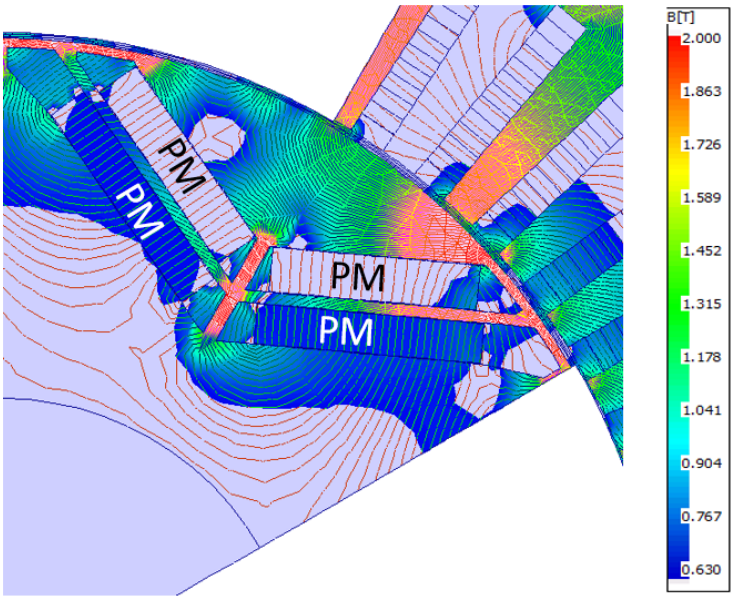

Figure 3. Evaluation of the demagnetization in the magnets.

2.2.4 Evaluation of KPIs (Key Performance Indicators)

During the different designs iterations, the following KPIs have been evaluated: (1) Power and torque density in the continuous service (Kw/Kg, Kw/l, Nm/Kg, Nm/l) and (2) rare earth savings with respect to motor benchmark. In section 6, the procedure to obtain these KPIs is explained.

3 PRELIMINARY SIZING OF THE MOTOR

Following the design procedure defined in Figure 1, first the 2D drawing of the stator has been defined. Then the rotor design has been accomplished.

3.1 Design Constraints

The number of pole pairs is set to $p = 3$ in order to limit the supplying frequencies. As it is well known, for a given mechanical speed, the higher the number of poles is the higher the supplying frequency is.

Multibarrier rotors are limited to 2 barriers due to manufacturability issues. The more barrier are the more magnets must be placed and the more complicated the assembling of the rotor is.

No skew is going to be implemented in order to simplify the rotor manufacturing (design to final cost reduction). Hence, new techniques for reducing the torque ripple are going to be implemented.

Wave winding technology must be implemented. The benefits of this technology against the conventional Hairpin will help accomplishing the KPIs.

The inner diameter of the stator is set to 134 mm in order to find a trade of between manufacturing issues at prototype stage and KPIs. In case of decreasing the stator inner diameter, extra tooling modifications should be needed in the continuous winding semi-automatic line. Otherwise, the manufacturing and assembly of the A+B prototypes in this semi-automatic line would not be feasible. This would have implied a risk of delaying the delivery times of the prototypes for A+B motors. On the other hand, higher diameters might increase notably the weight of the stator, decreasing the power and torque densities.

The stack length of the motor is defined as degree of freedom. However, from a preliminary approach it might be deduced that the stack length must be in the range of $65\ mm \div 70\ mm$ in order to reach the power density KPI.

The oil cooling system is going to be implemented. The heat is going to be extracted from the rotor by means of a through core cooling solution, and from the end windings by means of a spray cooling technology. It is expected that a maximum current density of $42\ A/mm^2$ can be affordable with this cooling system.

The magnets grade to be used in the design is the N38H. The benchmark motor uses higher thermal grade magnets. By decreasing the thermal grade, less content of HREE is required, and this will help to accomplish the REE saving KPI.

The thermal class of the stator windings is Class H (180ºC). Thus, the typical thermal class in electric vehicles is adopted.

Geometry	Pole Pairs	3
	Stator ID	134 mm
	Airgap	0.8 mm
Active Parts	Rotor Skew Angle	No Skew
	Electrical Steel Grade	NO 27
	Magnet Grade	N38H
	Cooling Circuit Design	Oil Cooling through rotor Spray oil cooling
Winding	Winding connections	3Y – Full Pitch
	eMotor thermal class	Class H (180ºC)
	Peak Current Density	42 A/mm^2

Table 1. Main Design Constraints

3.2 Design of the Stator

Once the number of pole pairs is established, there are constraints for configuring the stator in the wave winding technology. In the Table 2 the feasible stator alternatives are summarized for the case of $p = 3$ pole pairs.

The stator consisting of 36 slots is discarded due to the intrinsic high torque ripple. The higher the number of slots is the more distributed the windings are and the smaller the torque ripple is.

The stator consisting of 72 slots is also discarded due to manufacturing limitations. 72 slots might be too much for the defined stator inner diameter.

Continuos winding possible configurations				
Q	Layers	Parallels	Nph	Symmetry
36	6	1	36	Strong
		2	18	Strong
	8	1	48	Strong
		2	24	Strong
	10	1	60	Strong
		2	30	Strong
	12	1	72	Strong
		2	36	Strong
72	6	1	72	Strong
		2	36	Strong
	8	1	120	Strong
		2	48	Strong
		4	24	Weak
	10	1	120	Strong
		2	60	Strong
54	10	3	30	Strong
	12	3	36	Strong/Weak
		1	108	Weak

Table 2. Feasible stator solutions for p=3

Then, the only feasible solution is the stator comprising $Q = 54$ slots. Following this way, there are 2 alternatives regarding the number of conductors or layers inside the slot. 12 layer / 1 parallel path is discarded for mainly two reasons. On one hand, the resulting number of turns per phase is too high. This could limit significantly the base speed of the motor. The alternative with 12 layers / 3 parallel path could be better than 10 layers/ 3 parallel paths regarding the number of turns per phase. The higher the number of turns per phase is, the higher the peak torque capability is. It is true that it has not a strong symmetry, but neither is completely weak symmetry. Taking into account the benefits and being aware of the risks as well, it has been decided to choose the alternative with 12 layers / 3 parallel paths.

As next step, the dimensions of the stator geometry are defined considering the following aspects:

- **Magnetic Saturation**: The teeth and the yoke must not be strongly saturated at the peak operation point. The dimensions of the teeth must be big enough to avoid local saturations. However, they must be minimized as much as possible in order to reduce the weight of the stator. The best compromise must be found.
- **Manufacturing aspect**: the ratio $width/height$ of the conductors should be in the range of $0.45 \div 0.55$. Otherwise, problems may arise during the rolling of the matt on the inner tool making the winding unfeasible

In the Figure 4 the defined 2D drawing of the stator is shown.

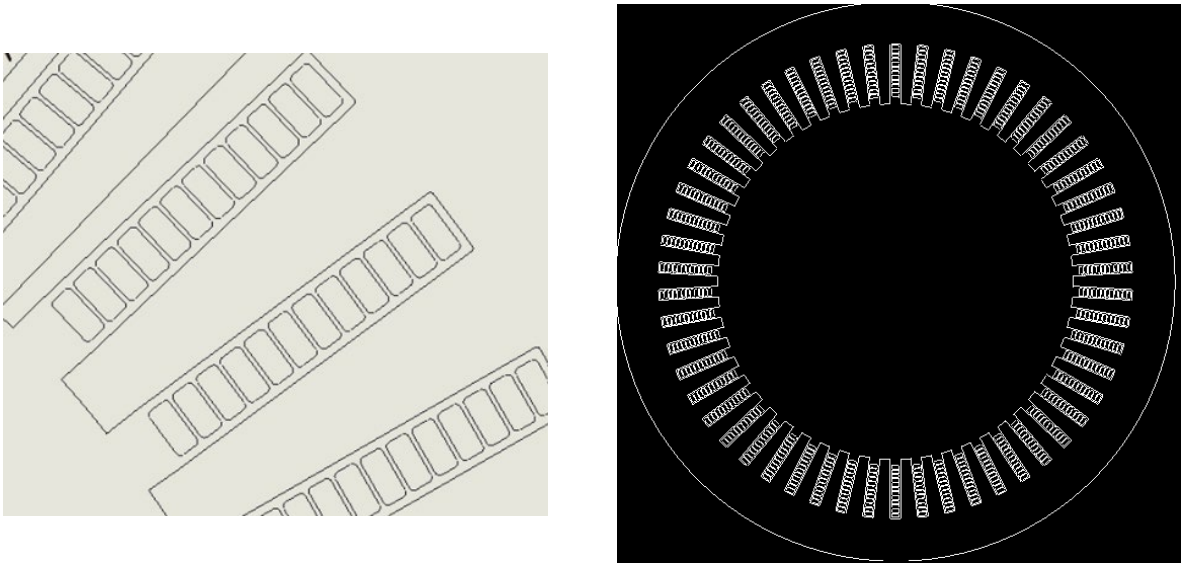

Figure 4. 2D drawing of the designed stator. 12 layers / 3 parallel paths

3.3 Design of the Rotor

Six different rotor layouts have been considered. These alternatives are described in the Figure 5.

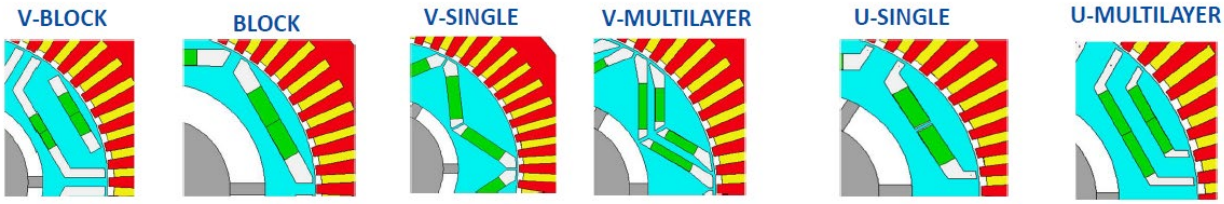

Figure 5. Different rotor layouts considered during the preliminary sizing stage

For each alternative the peak and continuous operating points are evaluated. The peak curve depends mainly on the magnetic design as the continuous operating point depends mainly on the thermal performance but also in the magnetic (losses + cooling system).

In order to reduce the mass of the active part as much as possible, the stack length is set to $70\ mm$ ($65\ mm$ is on the lower limit and might affect the manufacturing feasibility). Once defined the stack length the dimensions of the rotor are defined manually considering the next criteria:

- **Magnet Volume**. For a given current value and a given stator configuration, the peak torque capability depends on the magnetic flux created by the magnets. The effectiveness of the magnets must be improved in order to achieve the maximum magnetic flux with the minimum magnet volume.
- **Working Temperatures**. The maximum temperatures are limited to 180ºC Copper and 120ºC magnets. The maximum continuous power must be achieved in order to maximize the power density
- **Demagnetization**. The risk of demagnetization can be modified acting upon the magnets heigh. The higher the heigh of the magnets is the stronger the magnets are against the demagnetization. A good trade-off between demagnetization and magnet volume must be found.

In the Table 3 the main performances of the 6 rotor layouts are summarized. Significant differences can be appreciated, especially in the reduction of magnet weight and in the demagnetization risk. However, no alternative has been discarded in this stage and all of them

have been optimized in the next design stage. It seems that the V Block rotor is the best one, due to the fact that it offers a very good compromise among all evaluated performance and KPIs. It can be observed that the maximum power density is reached with the Block and U Single layouts, but there are rather weak against the demagnetization, especially the Block layout.

Rotor Topology	Motor Weight (kg)	Continuous Power Density (kW/kg)	Maximum Power (kW)	Magnet Weitht (kg)	Reduction in Magnet Weight (%)	Demagnetization (%) @Worse Peak WP2 at 120ºC	Demagnetization (%) @ID=300A at 120ºC	Efficiency (%) @WP2 in continuous
V + BLOCK	14.18	7.40	175	0.82	41%	0%	0%	89.6
BLOCK	13.75	7.79	179	0.88	37%	0%	75%	89.7
V SINGLE	15.11	6.51	164	0.98	30%	0%	100%	89.4
V MULTILAYER	14.10	7.78	183	0.96	32%	0%	47%	89.5
U SINGLE	14.32	6.91	165	0.90	35%	0%	14%	90.0
U MULTILAYER	17.95	5.61	168	0.81	42%	0%	0%	89.7

Table 3. Main performances of the 6 rotor layouts after the preliminary sizing

In the Figure 6 the resulting torque and power peak envelop for the V-Block rotor layout are plotted. It can be seen how the peak torque specification is fulfilled in all operating range, having especially big margin at high speed. This is because the base speed is situated much far from the value required by the application. As a consequence, the peak power capability of the motor is much higher than that required by the application.

In the Figure 7 the operation of the magnets at the working point WP1 is shown. The results are obtained for a magnet temperature of 120ºC. As it can be observed, the operating point of the magnets is set above the knee point (situated at 0.369T) around all the magnet regions. Hence, it can be stated that there is not any risk for the magnets to be demagnetized.

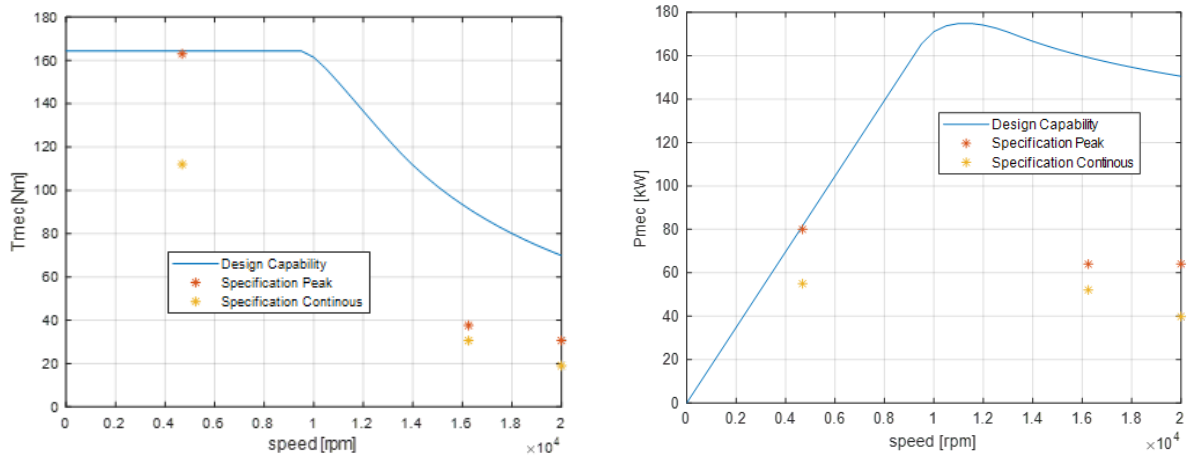

Figure 6. Torque and Power peak envelopes for the V-Block rotor layout

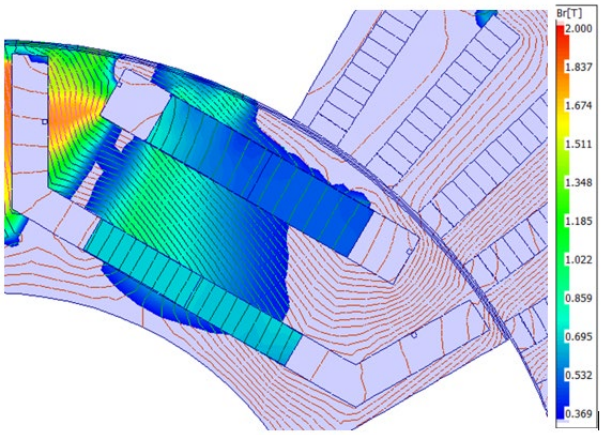

Figure 7. Operating point of the magnets at the working point WP1 (4688 rpm / 163 Nm) / 120ºC in the V-Block rotor layout

4 OPTIMIZATION OF THE ROTOR

After defining the preliminary rotor designs, the next stage focuses on design optimization (see the applied design methodology in Figure 1). As aforementioned, in this final design stage the 6 rotor altenatives are included. Eventhough some of them do not offer very promising results in the previos stage, they are no discarded until the end of the process.

4.1 Definition of the optimization process

Two optimization strategies have been defined, establishing different optimization objectives (see Table 4). In all cases, the same constraints have been defined. In the second strategy an additional objective regarding the magnet mass is included.

	Objectives	Constraints
Strategy 1	Maximize Power Density Minimize demagnetization @id=300Arms	Max magnet mass <1Kg Meet torque-speed requirement with 300Arms
Strategy 2	Maximize Power Density Minimize demagnetization @id=300Arms Minimize the magnet volume	Max magnet mass <1Kg Meet torque-speed requirement with 300Arms

Table 4. Definition of the optimization objectives and constraints.

In order to reduce the computational load and accelerate the optimization process the mechanical power computed at the base speed is considered to be maximized. Actually, this is not the maximum power along the peak envelop but it could be a valid reference for the optimization process. Computing exactly the maximum power value in each iteration leads to higher computational load.

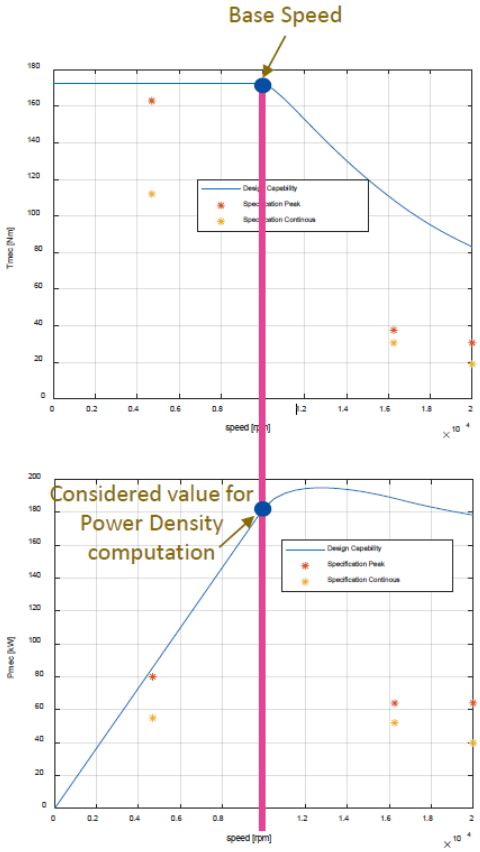

Figure 8. Mechanical power at base speed considered as the maximum power in the optimization process

4.2 Paretos of the optimization process

In next figures the optimization Pareto's of the considered rotor layouts are shown. At the end of the optimization process, two candidates are identified from the Pareto. The green point represents the candidate with maximum power density and without demagnetization. The pink one represents the maximum power density with a tolerance of 1.5% of energy loss in the magnets. Among these two candidates the one that considers a tolerance of 1.5% in the energy loss is chosen.

It must be underlined that the computed maximum power densities in all cases are slightly smaller than the real ones due to the fact that during the optimization process the power densities are calculated considering the power values at base speed (slightly smaller than actual maximum values). Hence, when the performances of all rotors are evaluated more in detail in the next section, the resulting power densities are sort of higher.

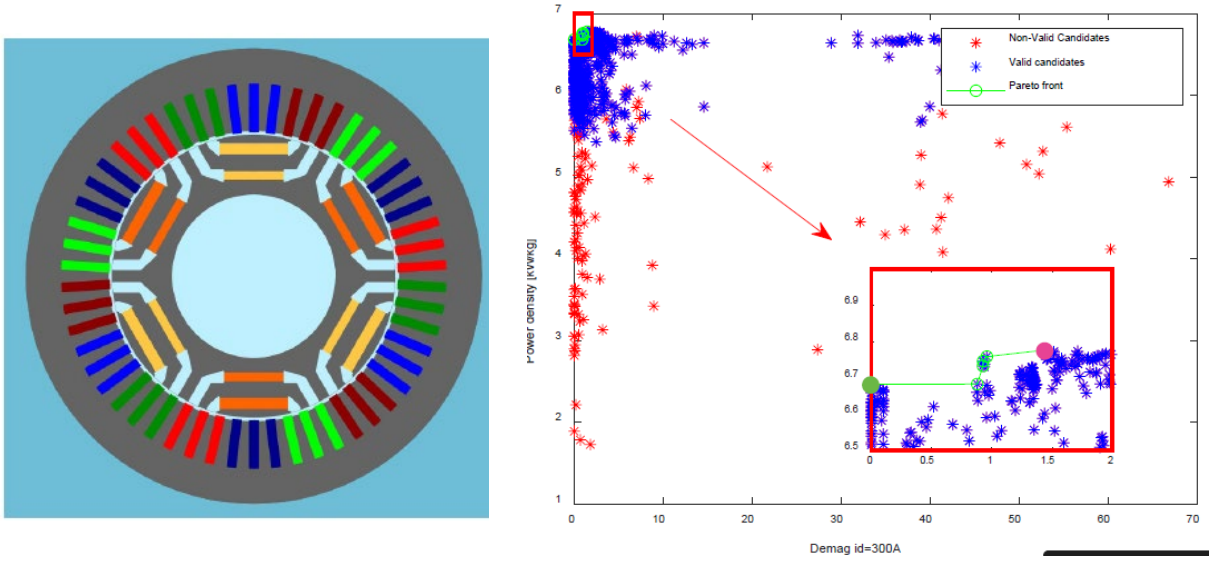

Figure 9. Optimization Pareto for the U-Multilayer rotor Layout (Max Power Density $6.78\ kW/kg$*). Optimization strategy 1*

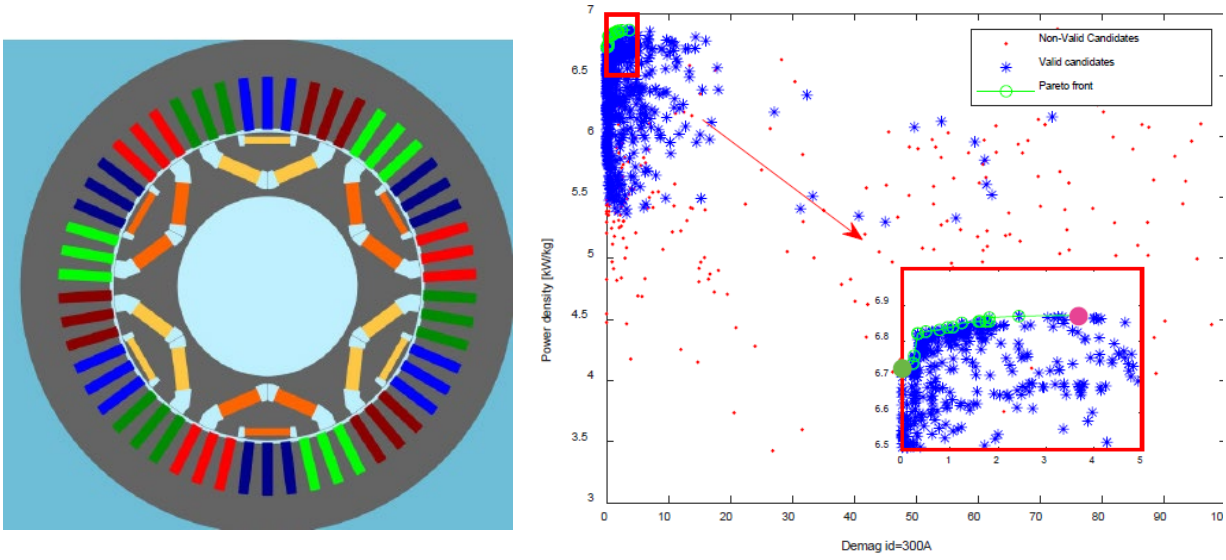

Figure 10. Optimization Pareto for the V-Block rotor Layout (Max Power Density $6.87\ kW/kg$*). Optimization strategy 1*

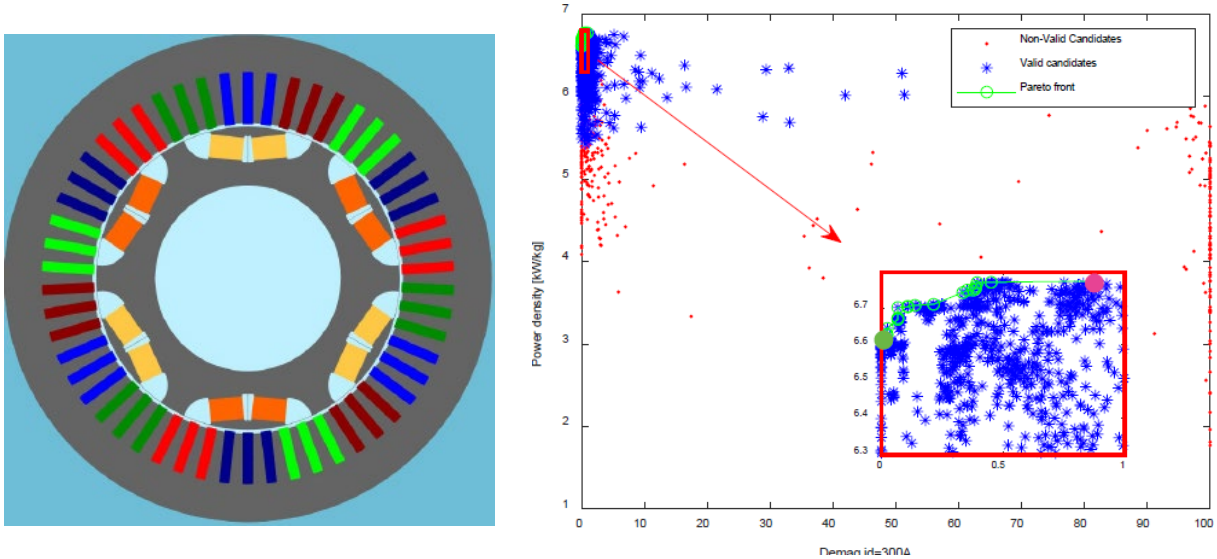

Figure 11. Optimization Pareto for the V-Single rotor Layout (Max Power Density $6.77\ kW/kg$*). Optimization strategy 1*

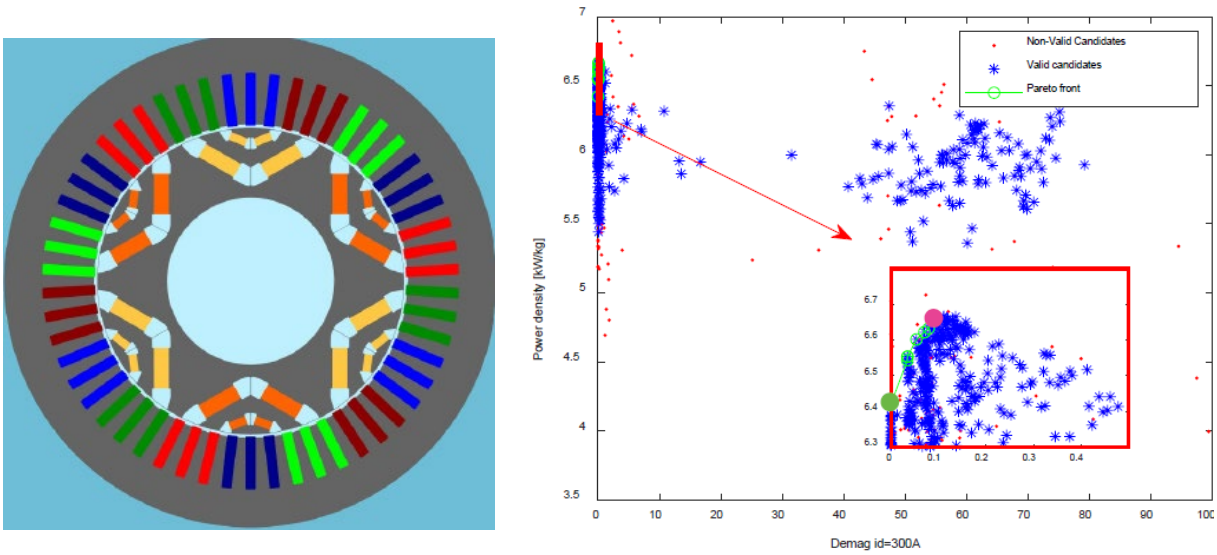

Figure 12. Optimization Pareto for the V-Multilayer rotor Layout (Max Power Density $6.67\ kW/kg$*). Optimization strategy 1*

The results obtained with the Block and U-Single rotor layouts are not shown, but their optimization processes have ended in the same results as in the case of the V-Single layout.

The final results obtained with the optimization strategy 2 have been the same as the ones obtained with the strategy 1. Thus, only the results obtained with the strategy 1 are reported in this section.

4.3 Performance and KPI analysis of optimized rotors

In next figures the main performances of optimized rotors are shown. All of them fulfil the peak torque requirement, actually with different margins, and there is not any risk of demagnetization at the working point WP1 in any of them.

In all cases it can be observed how the power density and torque density are sort of improved during the optimization process. On the contrary, the REE saving KPI is slightly decreased after the optimization. However, the REE KPI is achieved in all designs.

	Power Density (Kw/Kg)	Torque Density (Nm/kg)	Demagnetization (%)	REE Saving (%)
Presized	6.32	33.94	0	65
Optimized	6.94	33.87	0.21	59

Evaluation of KPIs

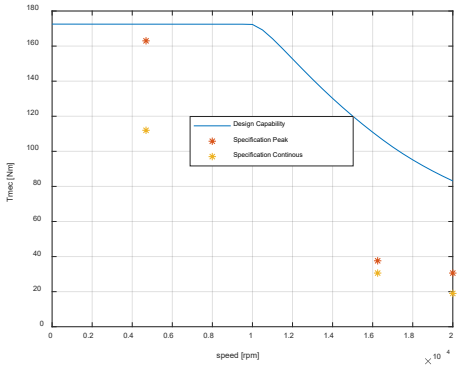

Peak torque

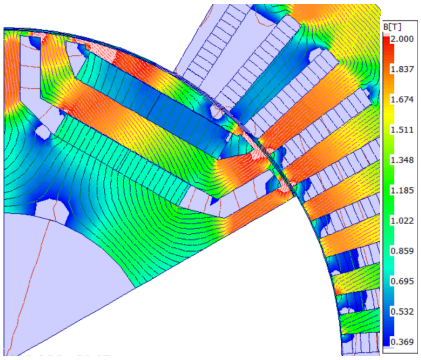

Magnetic Field Map at WP1

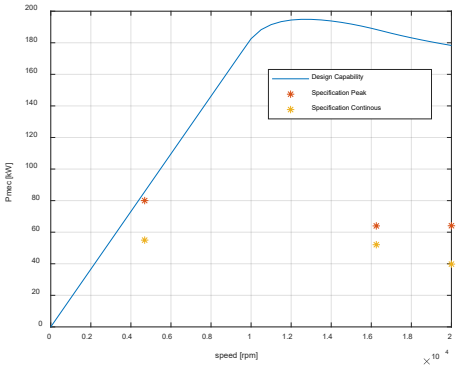

Peak Power

Figure 13. Performances of the optimized U-Multilayer rotor

	Power Density (Kw/Kg)	Torque Density (Nm/kg)	Demagnetization (%)	REE Saving (%)
Presized	6.53	34.62	0.33	62
Optimized	7.02	33.8	0.17	60

Evaluation of KPIs

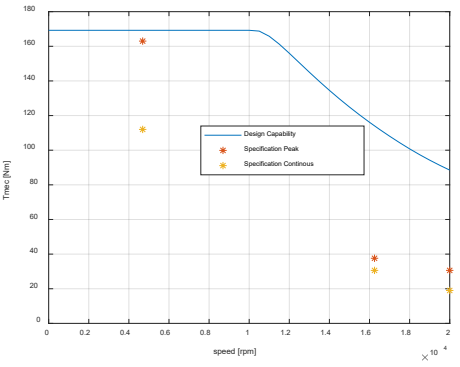

Peak torque

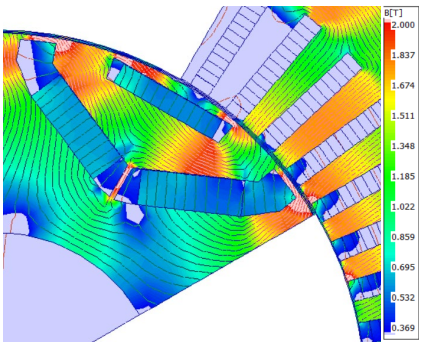

Magnetic Field Map at WP1

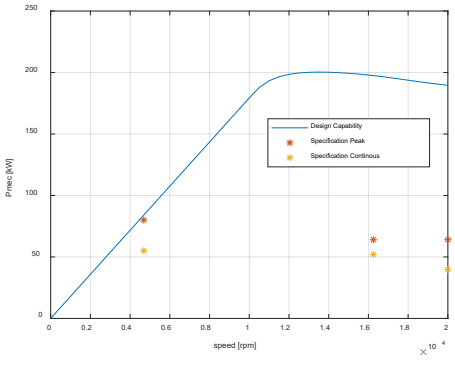

Peak Power

Figure 14. Performances of the optimized V-Block rotor

	Power Density (Kw/Kg)	Torque Density (Nm/kg)	Demagnetization (%)	REE Saving (%)
Presized	6.72	33.94	0.53	50
Optimized	6.87	33.82	0	59

Evaluation of KPIs

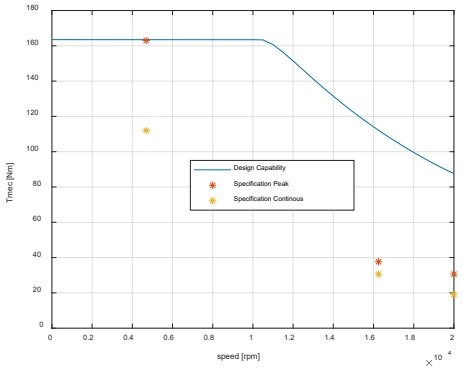

Peak torque

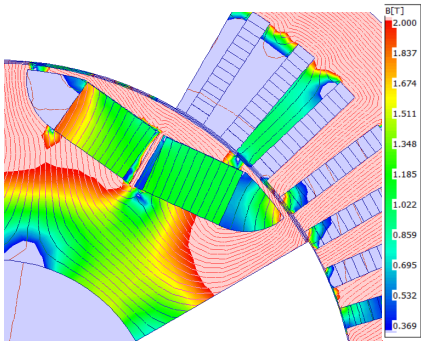

Magnetic Field Map at WP1

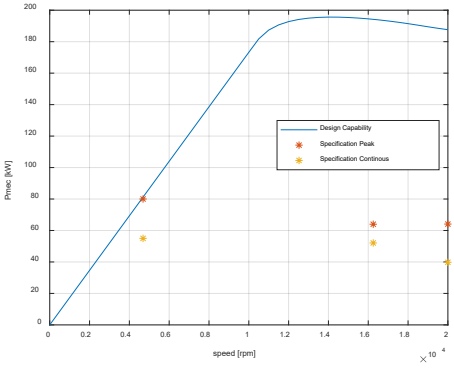

Peak Power

Figure 15. Performances of the optimized V-Single rotor

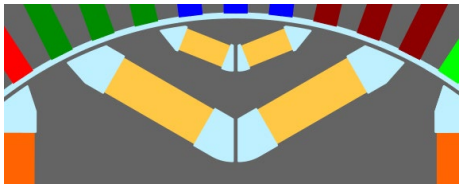

Evaluation of KPIs

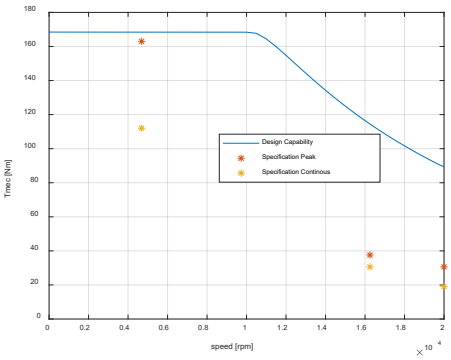

Peak torque

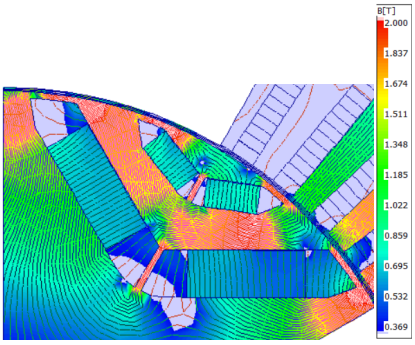

Magnetic Field Map at WP1

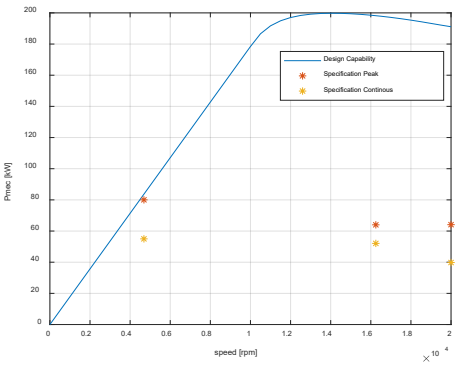

Peak Power

Figure 16. Performances of the optimized V-Multilayer rotor

In Figure 17 the summary of main KPIs is shown for all optimized rotor layouts applying the two optimization strategies. All of them achieve the torque density KPI (requirement $> 20\ N/kg$). Concerning the REE saving, all of them are practically on the specified value of 60%. However, it is completely fulfilled by the V-Block layout. Regarding to the risk of demagnetization, all of them are robust enough so that it can be stated that there is not any demagnetization risk. Finally, all candidates are very close to the specified minimum power density ($> 7Kw/Kg$), but only two of them, V-Block and V-Multilayer fulfil it.

Summarizing, although all rotor candidates are close to fulfil all KPIs and requirements, the V-Block alternative is chosen, mainly due to the next reasons:

- It is the only one that accomplish all KPIs and specificized performances
- It is the most robust structure regarding the mechanical performances

		No Gearbox		With Gearbox				Optimization Strategy 1	
Rotor Topology	Maximum Power (kW)	Motor Weight (kg)	Continuous Power Density (kW/kg)	Motor Weight (kg)	Continuous Torque Density (Nm/kg)	Magnet Weitht (kg)	REE Saving (%)	Demagnetization (%) @Worse Peak WP2 at 120ºC	Demagnetization (%) @ID=300A at 120ºC
U MULTILAYER	197	17.03	6.94	44.64	31.48	0.97	59%	0%	0%
V BLOCK	200	17.13	7.02	44.74	31.27	0.95	60%	0%	0%
V SINGLE	196	17.10	6.87	44.71	33.82	0.98	59%	0%	0%
V MULTILAYER	200	17.06	7.03	44.67	33.85	0.98	58%	0%	0%

		No Gearbox		With Gearbox				Optimization Strategy 2	
Rotor Topology	Maximum Power (kW)	Motor Weight (kg)	Continuous Power Density (kW/kg)	Motor Weight (kg)	Continuous Torque Density (Nm/kg)	Magnet Weitht (kg)	REE Saving (%)	Demagnetization (%) @Worse Peak WP2 at 120ºC	Demagnetization (%) @ID=300A at 120ºC
U MULTILAYER	202	17.24	7.02	44.85	31.93	0.98	58%	0%	0%
V BLOCK	200	17.10	7.02	44.71	31.76	0.96	59%	0%	0%
V SINGLE	199	44.84	6.92	44.84	33.72	0.99	58%	0%	0%
V MULTILAYER	197	17.13	6.89	44.74	33.80	0.97	59%	0%	0%

Figure 17. Summary of KPIs for all optimized rotor layouts, applying optimization strategies 1 & 2

4.4 Minimization of torque ripple in the V-Block rotor

Once the V-Block rotor has been chosen as the best candidate, it is modified in order to reduce the torque ripple. According to the internal specifications, the torque ripple must be below $\pm 5\%$ over the peak envelop working points (WP1. WP2, WP3). This internal specification is not mandatory, but it is considered this low torque ripple as a conservative guarantee to have a low NVH levels in the full eDrive system.

The torque ripple has not been considered as an optimization objective in the optimization process, so that the resulting torque ripple is above the specified maximum value. Thus, different design solutions have been evaluated in order to accomplish the torque ripple requirement. Finally, the adopted solutions have been the addition of magnetic wedges in the slot opening area, the adjustment of the pole span and the pole shifting.

The main torque ripple component is due to the effect of slots. Wave winding technology requires the slots to be completely open. This increase considerably the effect of the slots on the air-gap magnetic field and in consequence on the torque ripple, mainly over the so-called cogging component, but also on the load torque ripple. In order to reduce this effect, semi-magnetic wedges can be placed in the slot opening area. In the Figure 18 the resulting torque ripple before and after adding magnetic wedges is reported. This design modification makes possible to reduce the torque ripple but the effect is not enough as the resulting torque ripple is yet far above from the specified maximum value. Thus, additional modifications must be addressed.

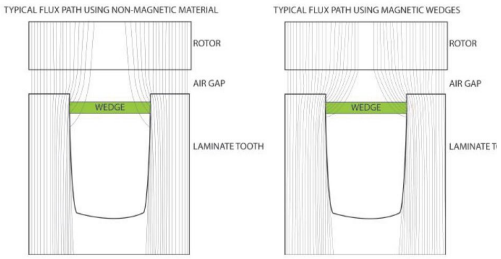

	Cogging	WP1	WP2	WP3
Original	±4 Nm	25%	58%	66%
Magnetic Wedge	±0 Nm	17%	30%	43%

Figure 18. Torque ripple reduction due to magnetic wedges

As a design constraint, in this case the rotor must not be skewed, so alternative solutions must be found to reduce the cogging torque. In this case, the pole shifting is proposed as an alternative design option. It consists of splitting the rotor in two parts and applying a shifting angle between the two parts, as it is depicted in the Figure 19. A very similar result of applying the skew is obtained with this design modification. As it is shown in the table integrated in the Figure 19, applying the pole shifting the cogging torque is completely removed, and the load torque ripple is considerably reduced, although not enough yet.

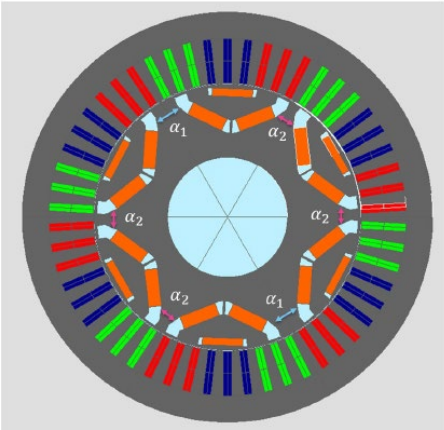

	Cogging	WP1	WP2	WP3
Original	±4 Nm	25%	58%	66%
Pole Shifting	±0 Nm	8%	13%	18%

Figure 19. Torque ripple reduction due to the pole shifting

In the Figure 20 the resulting torque ripple after adjusting the pole span is summarized. It can be seen that adjusting the pole span angle the torque ripple can be considerably reduced, but it is still above the defined maximum ripple value.

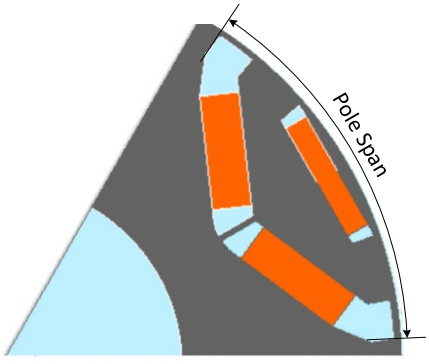

	Cogging	WP1	WP2	WP3
Original	±4 Nm	25%	58%	66%
Pole Span	±0.9 Nm	7%	18%	16%

Figure 20. Torque ripple reduction due to the pole span adjustment

Another design alternative considered in the study consist in modifying the shape of the rotor in order to obtain non-uniform airgap, but sinusoidal airgap. Sinusoidal airgap might eliminate some harmonics of the spectrum of the magnetic field in the airgap, and it should improve the torque ripple. The obtained results are shown in the Figure 21. The torque ripple is decreased a bit, but

perhaps not as much as expected. In addition, sinusoidal airgap distribution does not affect only to high order harmonics of the airgap magnetic field, but also to the fundamental harmonics, leading to a considerable decrease in the average torque. Due to that, this design alternative has been discarded.

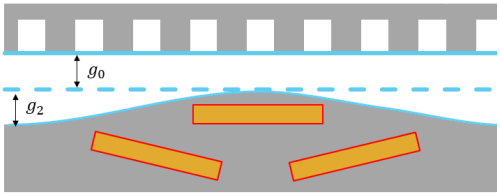

	Cogging	WP1	WP2	WP3
Original	±4 Nm	25%	58%	66%
Sinusoidal Airgap	±2.9 Nm	19%	33%	59%

Figure 21. Torque ripple reduction due to sinusoidal airgap

The considered design modifications individually are not enough to reduce the torque ripple below the specified maximum value. Hence, their combination has been analysed. In the Table 5 the obtained results are summarized. Combining the pole span adjustment and the pole shifting is enough to accomplish the torque ripple requirement, as the torque ripple is below 7% along all working points. Additionally, the torque ripple at different load situations has been also evaluated for this combination (see Figure 22). This performance is evaluated at the speed corresponding to the working point WP1 (4688rpm) and at different load situations. It can be seen that the resulting torque ripple is below the specified value practically in all cases, unless the 1% load situation. But this load operation is very restrictive so it can be stated that the obtained performance is really very good.

As aforementioned the stator geometry consist of completely open slots. That means that some additional pieces must be inserter in the base of the slot in order to fix the conductors inside the slot. This can be done with semi-magnetic pieces, and this way additional improvement of the torque ripple can be achieved. Thus, finally the three design options (magnetic wedge + pole span adjustment + pole shifting) are included, and the obtained torque ripple is very low (see Table 5).

Torque Ripple	Cogging	WP1	WP2	WP3
Original	±4 Nm	24%	58%	66%
Pole Span + Shifting + Magnetic Wedge	±0 Nm	2%	5%	5%
Pole Span + Shifting	±0 Nm	4%	7%	7%
Pole Span + Magnetic Wedge	±0.5 Nm	5%	12%	10%

Table 5. Resulting torque ripple with different design combinations

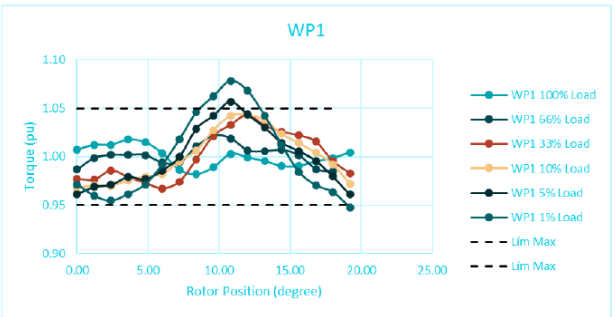

Load	I (A)	Angle (º)	Tav [Nm]	Tripple (Nm)	Tripple (%)
100%	300	55	164	6	4
66%	200	53	119	5	4
33%	100	42	60.8	4.6	8
10%	30	23	15.8	1.2	8
5%	15	15	7.4	0.71	10
1%	3	4	1.43	0.19	13

Figure 22. Torque ripple for the combination of pole span adjustment with pole shifting, at the speed corresponding to the WP1 and at different load situations

5 CONTINUOUS SERVICE PERFORMANCE

In this section the continuous service of the designed motor is evaluated. The maximum value of the continuous power and torque curves are used to compute the power and torque density KPIs. The continuous service characteristics depends on the thermal performances, which depends on the effectiveness of the cooling system and the losses of the electrical motor.

In this chapter, first the overall losses of the electrical motor are evaluated, and then these losses are introduced to the thermal simulations in order to evaluate the thermal performance of the motor. This way the continuous service characteristic is obtained.

5.1 Computation of losses

The losses are computed considering PWM voltages. A time step simulation of the motor is carried out in MATLAB-SIMULINK and the steady-state current waveforms are obtained at each working point. Then this current waveform is used to drive the FEA simulation and the overall losses of the motor are computed. The motor model used in time step simulations is based on flux maps defined by FEA simulations of the motor. This procedure is depicted in the Figure 23.

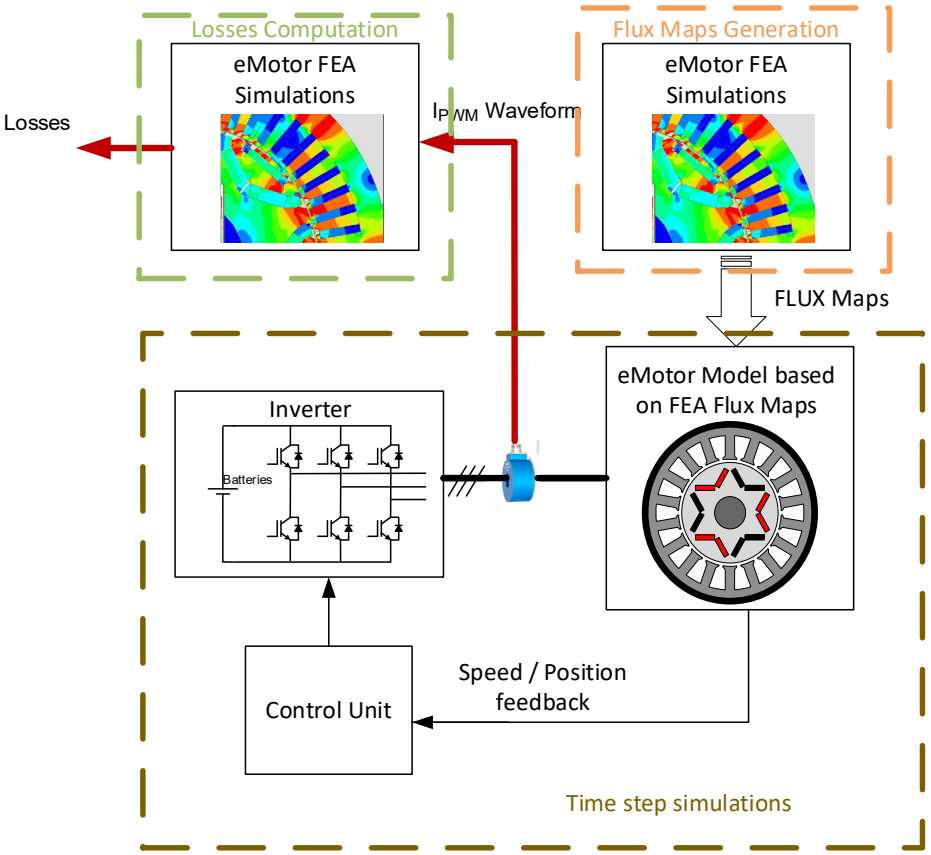

Figure 23. Procedure for losses computation accounting for PWM voltages

5.1.1 Copper losses

In low frequency operation the so-called AC copper losses are neglectable but at high frequencies these losses might be taken into consideration. In this case the operating frequencies might reach up to 1000 Hz. At this level the skin and proximity effects arise, and AC losses might become relevant. As it is shown in the Figure 24, at the maximum operating speed the total copper losses might increase 150% due to the effect of AC losses. This resistance increase is because a non uniform distribution of the current in the conductors, which become more relevant at high frequencies and is due to skin and proximity effects. This effect can be appreciated in the Figure 25.

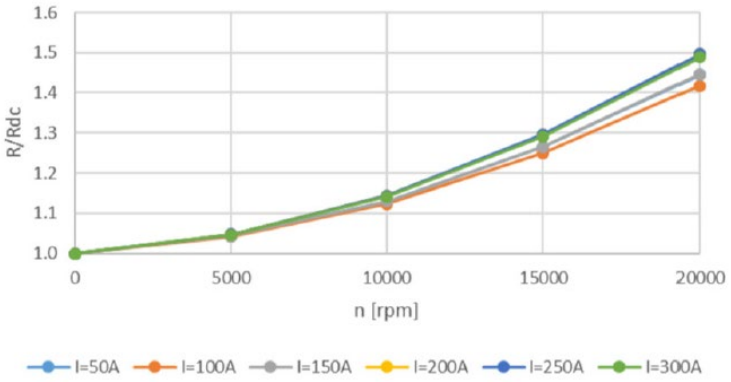

Figure 24. Variation of the effective resistance due to the effect of the frequency

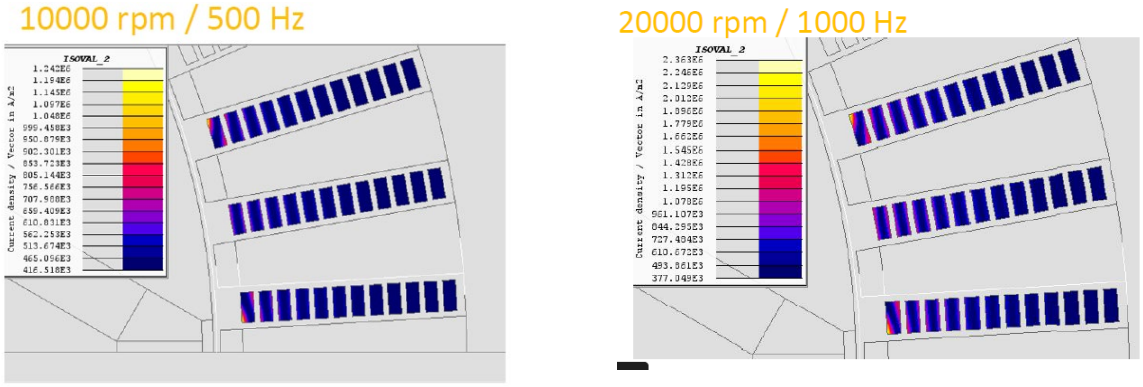

Figure 25. Effect of the frequency on the current distribution in the conductors

5.1.2 Iron losses

The iron losses are computed using the widely known Bertotti's model. The total iron losses are exploited in three components: hysteresis losses, Eddy losses and Excess losses. Each component is modelled by an analytical expression than involves a constant as it is described in the next equation

$$P_{iron} = K_h B^2 + K_e \left(\frac{dB}{dt}\right)^2 + K_{exc} \left(\frac{dB}{dt}\right)^3 \quad (1)$$

These constants must be adjusted for each electrical steel grade, based on experimental data provided by the supplier. In this project the electrical steel of grade NO27 is used. In the Figure 26 the adjusted Bertotti's model results are shown, and the values considered for the different coefficients are given as well.

The iron losses are multiplied by a factor of 3.62 in order to account for the effect of manufacturing process. Stamping, stacking and welding process might increase the theoretical iron losses. In this way, the additional losses due to manufacturing issues are taken into account.

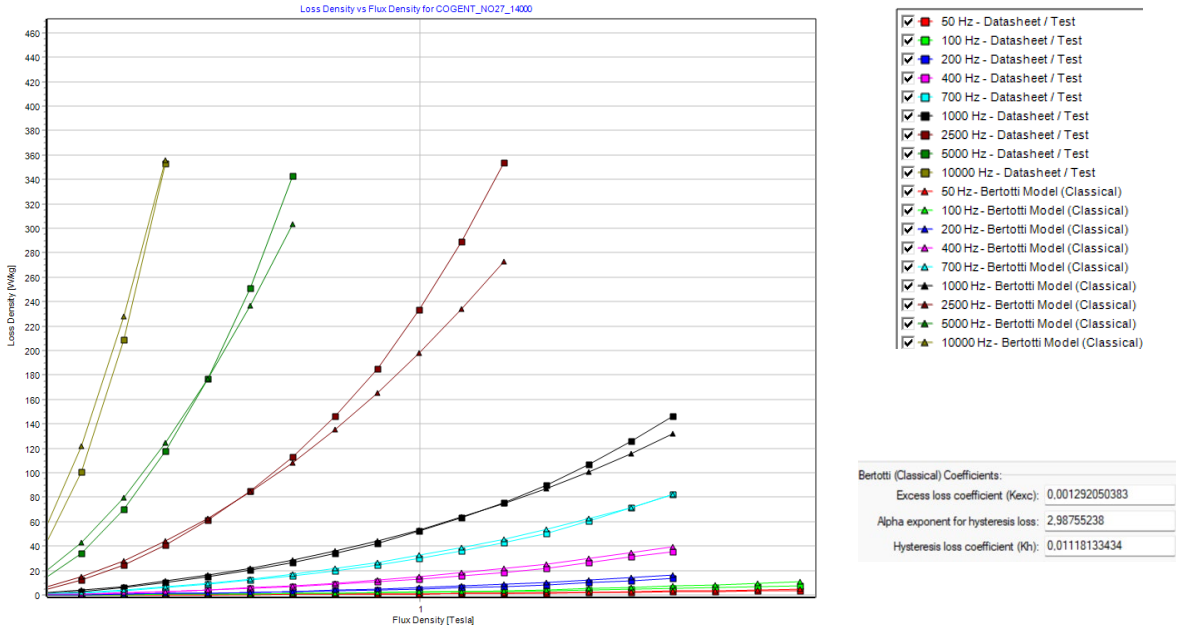

Figure 26. Comparison between experimental losses vs Bertotti's model losses for the electrical steel NO27

5.1.3 Magnet losses

Losses in the magnets occurs due to the induced eddy currents. The magnetic field seen by the magnets is mainly constant. However, there are some high frequency harmonics on the magnetic field crossing the magnets, created by the effect of stator slots and by high frequency current harmonics originated by PWM voltages. This alternating magnetic fields induce electromotive forces in the magnets. And as the magnets have conduction properties (they are not electrically isolated materials, but they have a resistivity) electric currents are induced. These induced currents generate losses.

The magnetic field crossing the magnets is precisely computed by FEA simulations performed in 2D at different load conditions. Then, considering the resistivity of the magnets the losses are computed from the magnetic field computed in FEA. The effect of magnet segmentation is considered by analytical approach. In this case, it is considered an axial segmentation. When segmenting the magnets, the losses are reduced notably.

It is remarkable that the losses computation in magnets involves rather uncertainty. Due to that, it is preferred to overestimate these losses, so a correction factor of 2 is adopted in the calculation.

5.2 Cooling system

The cooling consists of two systems: oil through rotor cooling and oil spray cooling.

A set of cooling channels are configured in the rotor. One channel through the shaft, and other channels on the sides of the inner layer of magnets as it is depicted in the Figure 27. The position of cooling channels close to the magnets is very important to improve the heat extraction from the magnets,

The spray cooling system is applied directly to the end winding. The majority of the heat generated in the copper is extracted via end windings.

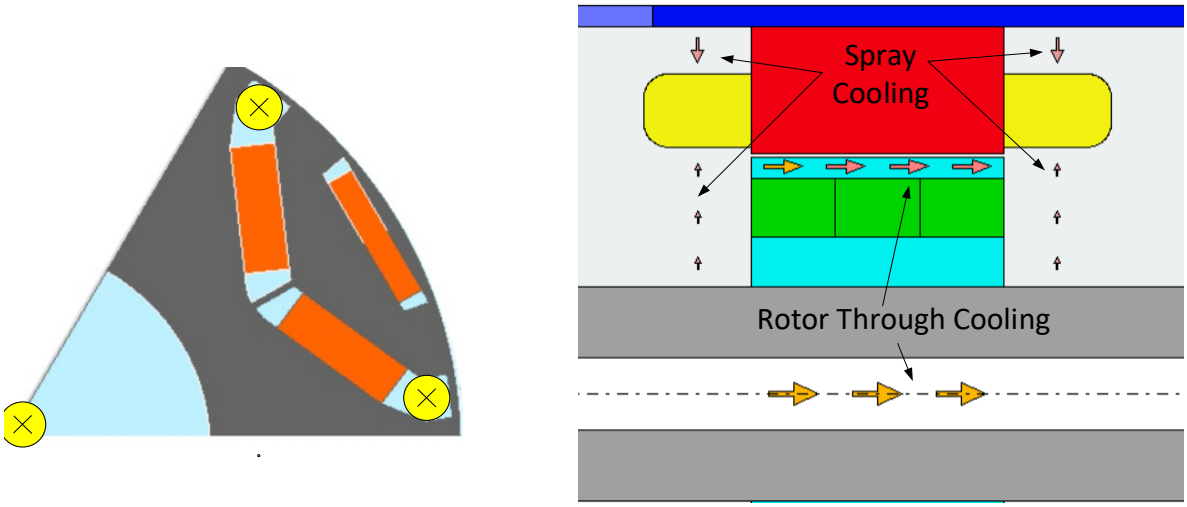

Figure 27. Description of the implemented cooling system

5.3 Continuous service curves

The continuous services curves are obtained in steady-state, limiting the working temperatures at 120ºC in case of magnets, and at 180ºC in case of windings.

For each working point many iterations must be performed until the final result is obtained. In the Table 6 the results are reported. Four working points are analysed. The three points defined in the specifications, and the working point corresponding to the maximum value of the power over the continuous service curve. This maximum point is located between the working points WP1 and WP2.

In the Figure 28 the continuous service curves for the power and the torque are shown. The maximum value of the power is about 127 Kw. This point is situated at the speed of 10500 rpm. Thus, the motor torque at this point is around 115.7 Nm. This power value is used for the computation of the KPI of power density. While the torque density KPI is computed using the axel torque, which is obtained multiplying the motor torque by the gearbox ratio.

	WP0	WP1	Pmax	WP2	WP3
Current [Arms]	350	340	215	113	86.53
Phase advance [º]	58.67	58.75	57	67.42	69.69
Speed [rpm]	1	4688	10500	16250	20000
Torque [Nm]	177.8	170.86	119.28	50.16	31.27
Torque Shaft Torque [Nm]	172.5	165.7	115.7	48.7	30.3
Power [kW]	0.0	81.4	127.2	82.8	63.5
Magnet temperature	90.52	119.3	120.5	120	119.2
Winding temperature	160.1	164.9	125.7	107	104.6
Copper dc	9868	9424	3402	891.6	519.3
Copper ac	12.69	302.8	734.9	375.3	320.8
Stator BI	0.03	287.2	685.8	654.7	636.6
Stator tooth	0.03	265.9	709.6	1374	1503
Magnet	0	51.53	93.96	139.7	127.4
Rotor pole	0.006	64.81	164.5	209.8	219.6
Rotor BI	0	1.893	4.06	4.4	9.18

Table 6. Continuous service working points computed in steady state

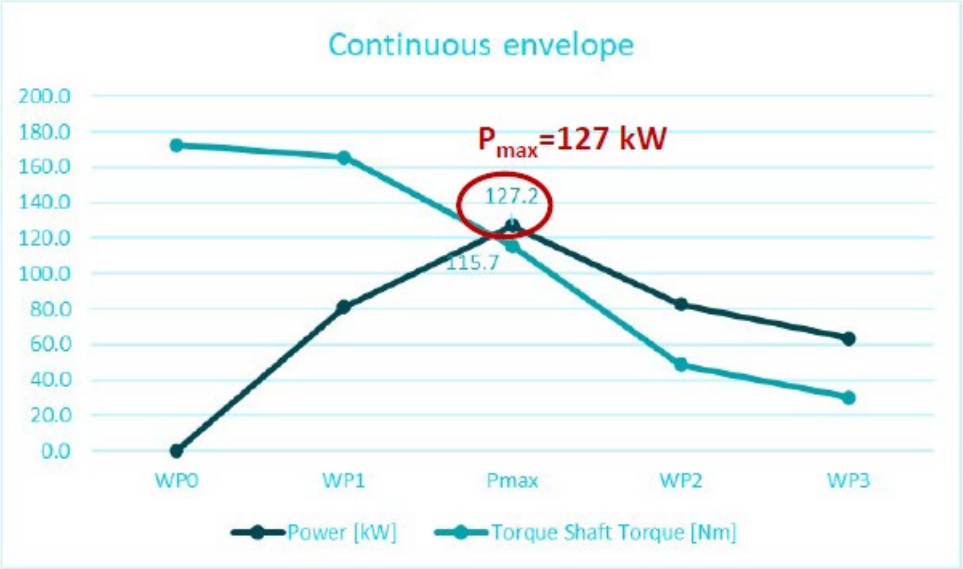

Figure 28. Continuous service curves

It is remarkable that at WP0 and WP1 the motor is able to provide the peak torque values in steady-state. In these operating points the rotating speed, and so the operating frequency are relatively low. Hence, the iron and magnet losses are rather small, and the cooling system is able to extract all the heat keeping the working temperatures below the maximum permissible values. In the working point WP1 the magnet temperature is practically the maximum. In the remaining working points at higher speeds, the iron and magnet losses increase significantly and the copper losses must be reduced (reducing the current, and so the torque) in order to avoid the overheating of the motor.

6 FINAL PERFORMANCES AND COMPUTATION OF KPIS

6.1 Evaluation of KPIs

In this section the evaluation of the KPIs is described. The reported values are the ones corresponding to the final AB segment motor design.

6.1.1 Computation of Weight and Volume

The weight of the electric motor is computed without and with gearbox. In the Figure 29 the considered dimensions and the elements considered as part of the motor and the ones considered as part of the gearbox are depicted. As the design of the gearbox is not part of the HEFT project scope, a base-line commercial gearbox is used to evaluate equivalent volume and weight. It should be noticed that the drawing of the gearbox (Figure 29) only represents the equivalent volume for the gearbox. Final gearbox geometries for a final integrated use are not defined. It should be mentioned that both bearings and the shaft are not considered as part of the electric motor, but as a part of the gearbox (as final gearbox will have an integrated mechanical frame with axle and bearings included)-

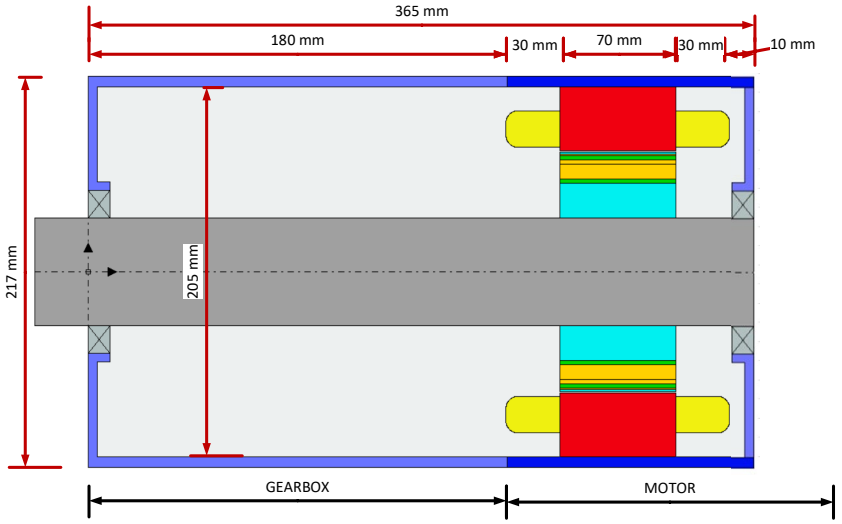

Figure 29. Main dimensions of the electric motor with a stack length of 70mm, including the gearbox

6.1.1.1 Gearbox

A commercial aluminium casing gearbox is included for the design and the front bearings and end cap are considered as part of the gearbox.

Volume	6.6 litres
Aluminium Casing Weight	4.3 kg
Total Weight	21.6 kg

Table 7. Considered weight and volume for the commercial gearbox

6.1.1.2 Stator and Rotor laminations Weight

The stator and rotor magnetic cores are made of silicon steel of grade NO 27. The density of the material is $7.6\ kg/dm^3$. Thus, the weight is computed multiplying the volume by the density. In the particular case of a stack length of $70\ mm$, the stator lamination weight is $7.175\ kg$ and the rotor lamination weight is $3.61\ kg$.

6.1.1.3 Copper Weight

The wave winding is characterized for having smaller end-windings than in conventional Hairpin. An end winding length of 30mm is considered. In the Figure 30 the estimation of the copper weight

is described. The end-winding contribution is considered constant, and the active weight is adapted to every stack length.

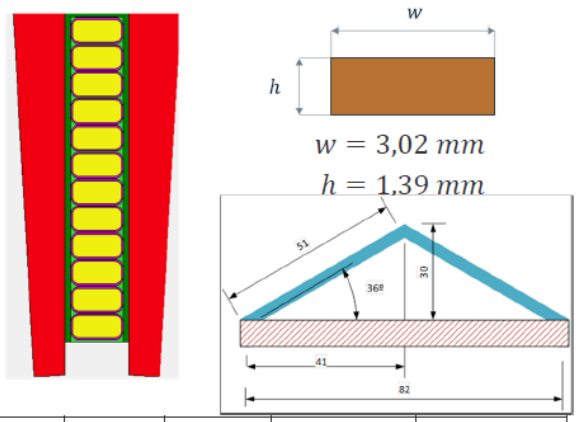

Stack length	Active Weight	End-Winding	Total Weight (Without fillet)	Total Weight (With fillet)
65 mm	1,584 kg	2,486 kg	4,07 kg	3,94 kg
70 mm	1,706 kg	2,486 kg	4,19 kg	4,06 kg

Figure 30. Estimation of the copper weight

6.1.1.4 Magnet Weight

The magnet grade is N38H. According to datasheets given by suppliers, this kind of magnets have a density of $7.5\ kg/m^3$. This way, the weight is computed multiplying the volume by the density. In the case of a stack length of $70\ mm$, the magnet weight is $0.949\ kg$.

6.1.1.5 Housing Weight

The housing is manufactured by SUMIBE's epoxy which have a density of $1.7\ kg/dm^3$. The width of the housing is set to $6\ mm$ and the length is about $185\ mm$, giving as a result a volume of $0.7358\ dm^3$, and a weight of $1.25\ kg$. These values correspond to a stack length of $70\ mm$.

6.1.1.6 Rear End Cap Weight

The rear end cap is manufactured by SUMIBE's epoxy which have a density of $1.7\ kg/dm^3$. The width of the end cap is defined to $5\ mm$. Hence, the volume of the rear end cap is $0.1436\ dm^3$, and the weight is $0.2442\ kg$. This value does not change with the stack length.

6.1.1.7 Rotor Cavity Weight

The rotor geometry has some holes. Some of them to situate the magnets, others for cooling purpose and others just to make the rotor lighter. In the assembly process of the rotor, the insertion of magnets inside the cavities requires the holes to be slightly higher and wider than the magnets. Once the magnets are put inside the cavities, fixing epoxy is injected so that all cavities are filled completely with this adhesive product. The employed epoxy has a density of $1.97\ kg/dm^3$. The weight of the fixing epoxy is also considered. In the case of the AB motor, the rotor cavity weight is 0.09 kg. Actually, the contribution with the fixing epoxy to the overall motor weight is practically neglectable. However, it has been included in the study.

6.1.1.8 Total motor Weight

In the Table 8 the estimated total weight of the electric motor without considering the gearbox is reported. The contribution of each element to the total weight is expanded.

Stator Lamination	7.18 kg
Rotor Lamination	3.61 kg
Armature Copper	4.06 kg
Magnet	0.95 kg
Housing	1.25 kg
End Cap Rear	0.24 kg
Rotor Cavities	0.09 kg
MOTOR WEIGHT (without gearbox)	17.39

Table 8. Estimated weight for the motor without gearbox (stack length of 70 mm)

Motor Weight without Gearbox	17.39 kg
Bearings Weight	0.66 kg
Shaft Weight	5.96 kg
Gearbox Weight	21.60 kg
TOTAL MOTOR WEIGHT (with gearbox)	45.60 kg

Table 9. Estimated total weight for the motor with gearbox (stack length of 70 mm)

6.1.1.9 Total motor Volume

The outer diameter of the motor considering the housing is $d_o = 217mm$. The length of the motor without considering the gearbox is $l_m = 140\ mm$. Hence, the total volume of the electric motor without considering the gearbox is:

$$V_{motor} = \pi \left(\frac{d_o}{2}\right)^2 \cdot l = \pi \left(\frac{0.217}{2}\right)^2 \cdot 0.140 = 5.18\ dm^3 \quad (2)$$

The overall volume of the motor is obtained adding the volume of the gearbox to the volume of the motor. The volumes are reported in the Table 10.

Gearbox Volume	6.6 litres
Motor Volume (without gearbox)	5.18 litres
Total Motor Volume (with gearbox)	11.78 litres

Table 10. Estimated overall volume of the electric motor with gearbox (stack length of 70 mm)

6.1.2 Evaluation of Torque and Power Densities

The power and torque density are computed considering the maximum values of torque and power in the continuous service. In case of the AB motor, the maximum value of the power in continuous service is $P_{cs-max} = 127\ kw$. And the maximum torque value in continuous service is $T_{cs-max} = 1562\ Nm$. The torque is computed at the output of the gearbox, so that it is actually the axis torque.

The power density is computed without considering the gearbox. It is calculated considering the weight and the volume.

$$P_{dens}\left(\frac{kw}{kg}\right) = \frac{P_{cs-max}}{W_{motor}} = \frac{127.2}{17.39} = 7.32\frac{kw}{kg}$$
$$P_{dens}\left(\frac{kw}{l}\right) = \frac{P_{cs-max}}{V_{motor}} = \frac{127.2}{5.18} = 24.57\ \frac{kw}{l} \quad (3)$$

The torque density is computed considering the gearbox. It is calculated considering the weight and the volume.

$$T_{dens}\left(\frac{Nm}{kg}\right) = \frac{T_{cs-max}}{W_{total}} = \frac{1562}{45.6} = 34.25\,\frac{Nm}{kg}$$
$$T_{dens}\left(\frac{Nm}{l}\right) = \frac{T_{cs-max}}{V_{total}} = \frac{1562}{11.78} = 132.62\,\frac{Nm}{l} \quad (4)$$

6.1.3 Evaluation of the REE Saving

The saving in rare earth elements is computed against the REE composition of benchmark magnets of grade N38H. The benchmark magnets have not Cerium so the light rare earth content is practically due to Neodymium. In the Table 11 the REE content of considered benchmark magnets is shown.

LREE (wt %)	26.1
Ce (%)	0
LREE_withoutCe (wt%)	26.1
HREE (wt %)	3.5
REE (wt %)	29.6

Table 11. REE composition of benchmark magnets of grade N38H

The composition of Cerium magnets is defined according to one best in class of the market. As it is shown in the Figure 31, currently N38H grade magnets can be achieved with a Cerium content in the range of 4%-8%. Cerium magnets of grade N38H have been analysed in the laboratory. The measured REE content is summarized in the Table 12.

LREE (wt %)	29
Ce (%)	7
LREE_withoutCe (wt%)	22
HREE (wt %)	1.5
REE (wt %)	30.5

Table 12. REE composition of benchmark magnets of grade N38H

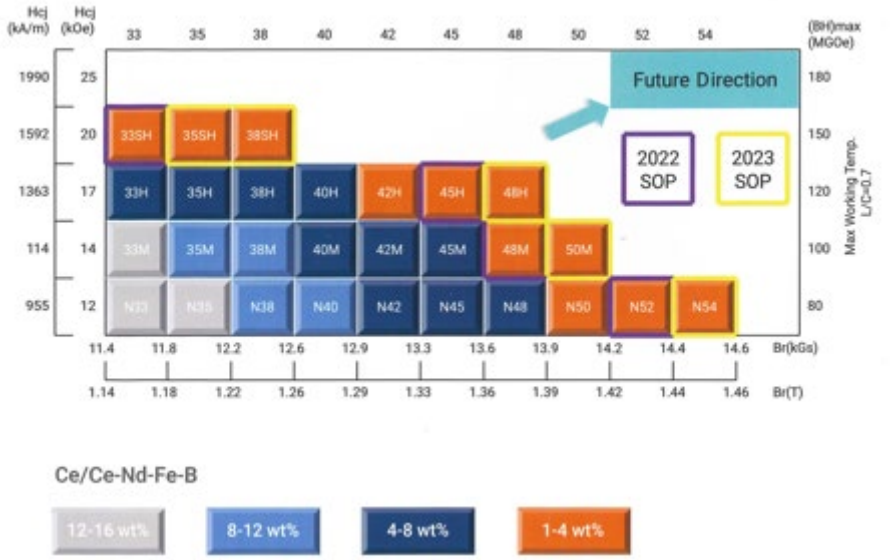

Figure 31. Cerium Magnet portfolio of one best in class in the market (Shanghai Sheensen Magnet Industry) [1]

Taking into account the contents reported in Table 11 and Table 12, the ratio in LREE is computed in the following way,

$$R_{LREE} = \frac{LREE_{Bestinclass}}{LREE_{Benchmar}} \cdot 100 = \frac{22}{26.1} \cdot 100 = 84.29\% \quad (5)$$

For that purpose, Cerium is not considered as LREE. In the same way, the ratio in HREE is computed as,

$$R_{LREE} = \frac{HREE_{Bestinclass}}{HREE_{Benchmar}} \cdot 100 = \frac{1.5}{3.5} \cdot 100 = 42.85\% \quad (6)$$

Up to this point, the ratio is computed accounting only to the chemical composition of the magnets. The addition saving due to the reduction of magnet weight is considered later. If the magnet weight is reduced in a ratio of R_{mw}, the ratio in LREE and HREE accounting for the weight reduction is calculated as follow,

$$RT_{LREE} = R_{LREE} \cdot R_{mw} = 84.29 \cdot R_{mw} \quad (7)$$

$$RT_{HREE} = R_{HREE} \cdot R_{mw} = 42.85 \cdot R_{mw} \quad (8)$$

The reference motor has 1.4 kg of magnets, whilst the AB segment motor has 0.949 kg. Hence, the magnet weight ratio between the AB segment motor and the reference motor is $R_{mw} = 67.78\%$. Thus, in this case the ratios result in,

$$RT_{LREE} = 84.29 \cdot 67.78 = 57.13\% \quad (9)$$

$$RT_{HREE} = 42.85 \cdot 67.78 = 29.04\% \quad (10)$$

The savings in REE is calculated as,

$$ST_{LREE} = 100 - RT_{LREE} = 42.87\% \quad (11)$$

$$ST_{HREE} = 100 - RT_{HREE} = 70.96\% \quad (12)$$

In order to obtain the REE saving, the weighted average value is calculated considering the savings in light and heavy rare earth elements. As it was defined in HEFT project grant agreement, weight of 40% is given to the LREE saving, and a weight of 60% is defined for the HREE saving. This way the total HREE saving factor is calculated,

$$REE_{saving} = 0.4 \cdot ST_{LREE} + 0.6 \cdot ST_{HREE} = 0.4 \cdot 42.87 + 0.6 \cdot 70.96 = 59.72\% \quad (13)$$

6.2 Final Perfomances

In this section the final performances of the AB segment motor design are reported. In the Figure 32 the resulting peak envelop of torque and power are plotted. It can be seen that the obtained working point at base speed is the required one, while at higher speeds the peak envelops are above the required values with a considerable margin.

In the Figure 33 the torque and power curves on continuous service are shown. Mention that in both cases, the motor capability is above of requirement in the overall speed ranges. These good performances in continuous services make possible to achieve the power and torque density KPIs.

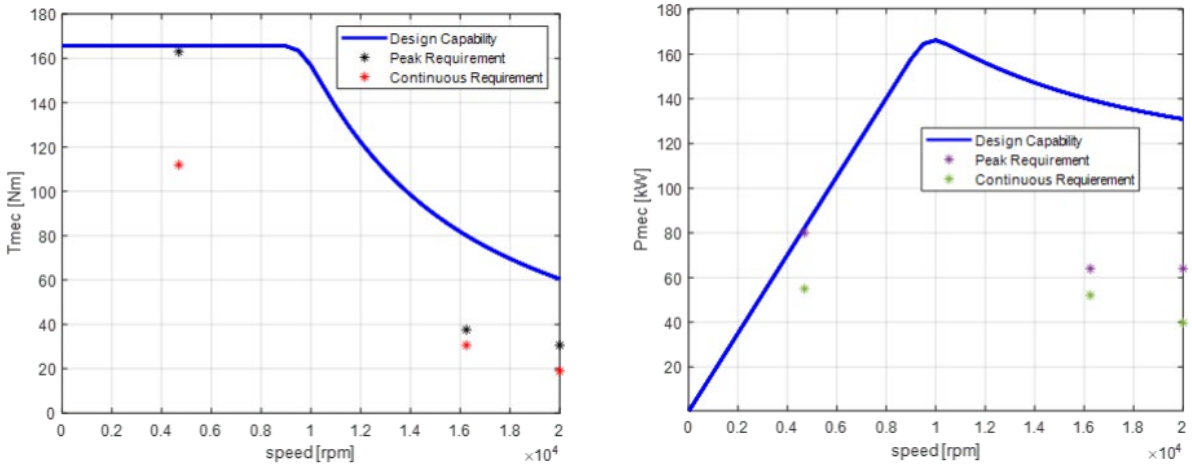

Figure 32. Peak envelope of mechanical torque and mechanical power

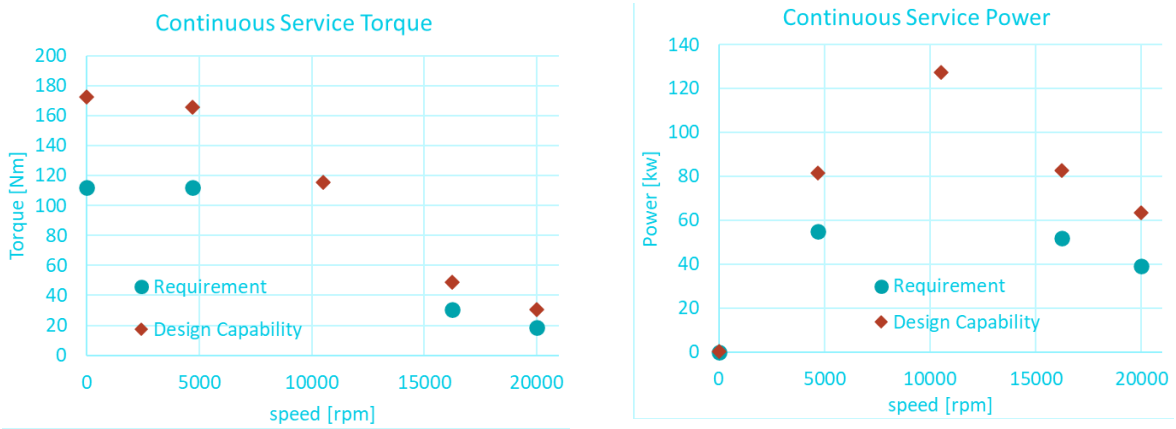

Figure 33. Continuous services curves for mechanical torque and mechanical power

Besides the main performance curves, in this chapter also the computed KPIs for the final motor design are reported. Underline that the proposed motor design fulfils all KPI's considering the

defined targets. Some differences appear from GA computations. These differences are mainly due to: (1) the maximum speed change from 25.000rpm to 20.000rpm and (2) the use of a larger stator inner diameter (semi-automatic winding line restrictions for continuous winding).

	Call Target	GA computations	Obtained Result
Power density (kw/kg)	$> 7\ kw/kg$	$\approx 8.39\ kw/kg$	$7.32\ kw/kg$
Power density (kw/l)	$> 23 kw/L$	$\approx 41.81\ kw/L$	$24.47\ kw/L$
Torque density (Nm/kg)	$> 20\ Nm/kg$	$\approx 35.84\ Nm/kg$	$34.25\ Nm/kg$
Torque density (Nm/l)	$> 50\ Nm/L$	Non-defined	$132.62\ Nm/L$
REE Saving	$> 60\%$	$\approx 63\%$	60%

Table 13. Final KPIs obtained with the eMotor design for segment AB

7 DELIVERY DEVIATIONS FROM THE INITIAL PLANNING

There has been a delay in the delivery of D4.1 Electromagnetic and Performance. Design Report of Motor for Class A+B Vehicles

Contractual delivery: 2024-05-31

Deliverable Date: 2024-07-24

Technical deviations:

This delay is due to the several iterations during the design of the emotor to have an emotor capable to be manufactured by wave winding in the automatic manufacturing line available at the University of Nottingham.

Delay effect on overall project planning:

The delay in D4.1 has no effect on the overall project planning. In M18 a first A+B motor design was obtained allowing to follow the manufacturing preparation activities in task 4.3 (as it was planned). The design iterations of A+B motor from M18 to M20 have been also used to apply iterative winding manufacturing trials allowing a good progress in task 4.3.

8 CONCLUSIONS

A new motor design for AB segment electric vehicles is reported in this document. The proposed motor design is characterized by a very high power density ($> 7\ kw/kg\ \ | > 23\ kw/l$), torque density ($> 20\ Nm/kg\ | > 50\ Nm/l$) and very low REE usage (REE saving $> 60\%$ in comparison with benchmark motors).

As main conclusion it can be stated that the proposed motor design fulfils all design requirements and KPIs defined in the call. These successful results have been possible thanks to the implementation of different novel technologies in the design of the motor: Wave windings, multibarrier IPM rotors, light epoxy materials and spray cooling.

Wave winding technology makes possible to perform very compact windings and also makes possible to insert 12 conductors inside the slot. The state of the art is about 8 conductors per slot with hairpin technology. Increasing the number of conductors inside the slots the AC losses are reduced, and more turns per phase are achieved. Increasing the number of turns per phase makes possible to reduce the required magnet flux, reducing this way the used magnet volume. Moreover, compact windings means that less copper is used leading to lighter stators.

The use of novel epoxy materials for the manufacturing of the housing makes possible to reduce considerably the weight of the housing, contributing to the consecution of the power and torque density KIPs.

The optimization of the multibarrier rotors makes possible to optimize the usage of magnets. This impact mainly to the REE saving KPI but also to the power and torque density. The less magnet weight is used, the lighter the rotor is.

The cooling channels situated near the magnets improve the heat extraction from the magnets. Moreover, the spray cooling applied over the end-windings enhances the direct heat extraction from the copper. With this cooling system rather high continuous service curves are achieved leading to high power and torque densities.

9 REFERENCES

[1] «Shanghai Sheensen Magnet Industry Co., Ltd,» 2024. [On-line. Access 2024-07-24]: https://www.xs-magnetics.com/en/advantage-152.html.